

## Energy dependence of particle multiplicities in central Au+Au collisions

B.B.Back<sup>1</sup>, M.D.Baker<sup>2</sup>, D.S.Barton<sup>2</sup>, R.R.Betts<sup>6</sup>, R.Bindel<sup>7</sup>, A.Budzanowski<sup>3</sup>, W.Busza<sup>4</sup>, A.Carroll<sup>2</sup>, J.Corbo<sup>2</sup>, M.P.Decowski<sup>4</sup>, E.Garcia<sup>6</sup>, N.George<sup>1</sup>, K.Gulbrandsen<sup>4</sup>, S.Gushue<sup>2</sup>, C.Halliwell<sup>6</sup>, J.Hamblen<sup>8</sup>, C.Henderson<sup>4</sup>, D.Hicks<sup>2</sup>, D.Hofman<sup>6</sup>, R.S.Hollis<sup>6</sup>, R.Holyński<sup>3</sup>, B.Holzman<sup>2</sup>, A.Iordanova<sup>6</sup>, E.Johnson<sup>8</sup>, J.Kane<sup>4</sup>, J.Katzy<sup>4,6</sup>, N.Khan<sup>8</sup>, W.Kucewicz<sup>6</sup>, P.Kulinich<sup>4</sup>, C.M.Kuo<sup>5</sup>, W.T.Lin<sup>5</sup>, S.Manly<sup>8</sup>, D.McLeod<sup>6</sup>, J.Michałowski<sup>3</sup>, A.Mignerey<sup>7</sup>, J.Mülmenstädt<sup>4</sup>, R.Nouicer<sup>6</sup>, A.Olszewski<sup>3</sup>, R.Pak<sup>2</sup>, I.C.Park<sup>8</sup>, H.Pernegger<sup>4</sup>, M.Rafelski<sup>2</sup>, M.Rbeiz<sup>4</sup>, C.Reed<sup>4</sup>, L.P.Remsberg<sup>2</sup>, M.Reuter<sup>6</sup>, C.Roland<sup>4</sup>, G.Roland<sup>4</sup>, L.Rosenberg<sup>4</sup>, J.Sagerer<sup>6</sup>, P.Sarin<sup>4</sup>, P.Sawicki<sup>3</sup>, W.Skulski<sup>8</sup>, S.G.Steadman<sup>4</sup>, P.Steinberg<sup>2</sup>, G.S.F.Stephans<sup>4</sup>, M.Stodulski<sup>3</sup>, A.Sukhanov<sup>2</sup>, J.-L.Tang<sup>5</sup>, R.Teng<sup>8</sup>, A.Trzupek<sup>3</sup>, C.Vale<sup>4</sup>, G.J.van Nieuwenhuizen<sup>4</sup>, R.Verdier<sup>4</sup>, B.Wadsworth<sup>4</sup>, F.L.H.Wolfs<sup>8</sup>, B.Wosiek<sup>3</sup>, K.Woźniak<sup>2,3</sup>, A.H.Wuosmaa<sup>1</sup>, B.Wyslouch<sup>4</sup>

(PHOBOS Collaboration)

<sup>1</sup> Physics Division, Argonne National Laboratory, Argonne, IL 60439-4843

<sup>2</sup> Chemistry and C-A Departments, Brookhaven National Laboratory, Upton, NY 11973-5000

<sup>3</sup> Institute of Nuclear Physics, Kraków, Poland

<sup>4</sup> Laboratory for Nuclear Science, Massachusetts Institute of Technology, Cambridge, MA 02139-4307

<sup>5</sup> Department of Physics, National Central University, Chung-Li, Taiwan

<sup>6</sup> Department of Physics, University of Illinois at Chicago, Chicago, IL 60607-7059

<sup>7</sup> Department of Chemistry, University of Maryland, College Park, MD 20742

<sup>8</sup> Department of Physics and Astronomy, University of Rochester, Rochester, NY 14627  
(June 6, 2006)

We present the first measurement of the pseudorapidity density of primary charged particles in Au+Au collisions at  $\sqrt{s_{NN}} = 200$  GeV. For the 6% most central collisions, we obtain  $dN_{ch}/d\eta|_{|\eta|<1} = 650 \pm 35(\text{syst})$ . Compared to collisions at  $\sqrt{s_{NN}} = 130$  GeV, the highest energy studied previously, an increase by a factor of  $1.14 \pm 0.05$  is found. The energy dependence of the pseudorapidity density is discussed in comparison with data from proton-induced collisions and theoretical predictions.

PACS numbers: 25.75.-q

Collisions of gold nuclei at an energy of  $\sqrt{s_{NN}} = 200$  GeV have been studied using the PHOBOS detector. PHOBOS is one of the experiments at the Relativistic Heavy-Ion Collider (RHIC) at Brookhaven National Laboratory aimed at understanding the behavior of strongly interacting matter at high temperature and density. Quantum chromodynamics (QCD), the fundamental theory of strong interactions, predicts that under these conditions, which may be probed in heavy-ion collisions, a new state of matter will be formed, the quark-gluon plasma (QGP) [1]. In this state, quarks and gluons are no longer confined inside hadrons, as is the case for normal nuclear matter. Information about the particle and energy density achieved in the early stages of the collision process is carried by the pseudorapidity density of particles emitted from the primary collision point [2]. In this analysis, we have determined the pseudorapidity density of charged particles,  $dN_{ch}/d\eta$ , in the most central Au+Au collisions. We focused in particular on the region near  $\eta = 0$ , where  $\eta = -\ln \tan(\theta/2)$  and  $\theta$  is the polar angle from the beam axis.

In combination with results from lower energies, these data permit a systematic analysis of particle production mechanisms in nucleus-nucleus collisions. Extension of

the energy range to  $\sqrt{s_{NN}} = 200$  GeV allows a study of the relative contributions of hard parton-parton scattering processes, which can be calculated using perturbative QCD, and soft processes, which are treated by phenomenological models that describe the non-perturbative sector of QCD. With increasing collision energy, hard processes are expected to become increasingly important for particle production near mid-rapidity.

For Au+Au collisions at RHIC energies, the yield and momentum distribution of particles produced by hard scattering processes may be modified by “jet quenching”, *i.e.* the energy loss of high momentum partons in the nuclear medium [3]. This phenomenon has been proposed as a diagnostic tool for characterizing the initial parton density in Au+Au collisions at these energies. Preliminary results indicate that in central Au+Au collisions at  $\sqrt{s_{NN}} = 130$  GeV the particle spectra at large transverse momenta, normalized to  $p\bar{p}$  collisions, indeed change in comparison with lower collision energies [4].

Early predictions for the charged particle pseudorapidity density varied by more than a factor of two, as shown in [5]. Data on the primary charged particle density  $dN_{ch}/d\eta|_{|\eta|<1}$  at energies of  $\sqrt{s_{NN}} = 56$  and 130 GeV [6] have been analyzed in a wide variety of theoretical models [7–14]. Generally, most models allowed a reasonable description of the energy dependence of  $dN_{ch}/d\eta|_{|\eta|<1}$  up to  $\sqrt{s_{NN}} = 130$  GeV, with suitable choices of parameters. For the ratio of particle densities near  $\eta = 0$  at 130 GeV and 200 GeV, most calculations predict an increase between 9 and 20%. An interesting exception is the model of Wang and Gyulassy [7]. When the effects of jet quenching are included in their calculation, they not only predict a suppression of particle spectra at high transverse momenta, but also a change of the energy

dependence of  $dN_{ch}/d\eta|_{|\eta|<1}$ , leading to an increase of more than 30% between 130 and 200 GeV when the default parameter set is used. The energy dependence of particle production presented here provides important constraints on this effect.

Details of the PHOBOS experimental setup can be found elsewhere [15,16]. The apparatus, shown schematically in Fig. 1, employs silicon detectors for vertex finding, particle tracking and multiplicity measurements. This analysis is based on the first 6 layers of the 16 layer two-arm spectrometer (SPEC), the two-layer vertex detector (VTX), the single-layer octagon barrel detector (OCT) and the three single-layer ring detectors (RING) located on either side of the interaction point. The acceptance of SPEC, VTX and OCT includes  $-1 < \eta < 1$ , covering different regions of azimuth. The combined acceptance of OCT and RING detectors reaches  $\eta = \pm 5.4$ . For the 2001 run period, 137168 silicon channels were read out, of which less than 2% were non-functional.

The detector setup also included two sets of 16 scintillator counters (“paddle counters”) located at  $-3.21$  m (PN) and  $3.21$  m (PP) relative to the nominal interaction point along the beam ( $z$ ) axis. These counters covered pseudorapidities between  $3 < |\eta| < 4.5$  and served as the primary event trigger. In combination with the zero-degree calorimeters at  $z = \pm 18.5$  m, which measured the energy deposited by spectator neutrons, PP and PN were also used for offline event selection.

Monte Carlo (MC) simulations of the detector performance were based on the HIJING event generator [17] and the GEANT 3.21 simulation package, folding in the signal response for scintillator counters and silicon sensors. In the calibration of the analysis methods we employed a particle selection procedure that allowed us to iteratively modify the MC output and optimize the agreement of the deposited energy distributions in data and MC.

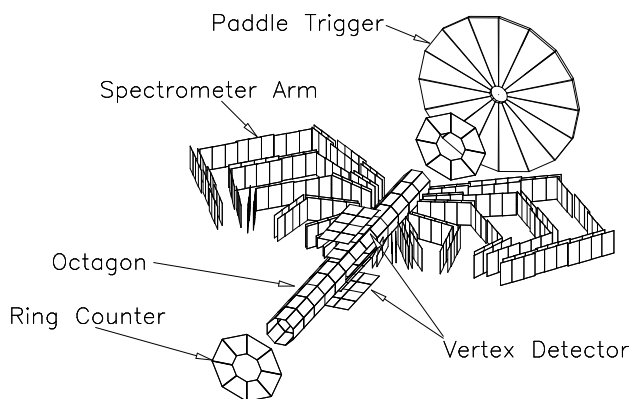


FIG. 1. Detector setup for the 2001 running period. Shown are the active elements of the detector systems used for this analysis. For clarity, one of the paddle counters and the two outer ring counters on each side were omitted and the positions of ring and paddle counters are not to scale.

Details of the trigger performance and the event selection procedure can be found in [6,18]. Based on MC simulations, we estimate that the trigger was sensitive to  $97 \pm 3\%$  of the total hadronic inelastic cross section. For the selection of central events used here, no contamination from beam-gas or other background collisions was found. The distribution of the combined signal from PP and PN (“paddle mean”) is shown in Fig. 2 for events with more than two hits in each paddle counter. This selection includes  $88 \pm 3\%$  of the hadronic cross section. We selected the top 6% of the total hadronic cross section with the largest paddle mean, corresponding to the most central collisions with the largest number of participating nucleons. Applying the 6% centrality cut to MC events, we deduce that the average number of participating nucleons in the data is  $\langle N_{part} \rangle = 344 \pm 10$  (syst). The systematic uncertainty was estimated using MC studies [18] and an analysis of the correlations between the signals in PN and PP.

For the selected central events, the event vertex was determined using the SPEC and VTX subdetectors. Details of the vertex finding procedure can be found in [6,18]. MC studies and correlations between the vertex positions found independently using SPEC and VTX detectors indicate a vertex resolution of better than  $400\mu\text{m}$  and a vertex finding efficiency of 100% in a fiducial range of  $-10 \text{ cm} < z_{vtx} < 10 \text{ cm}$ . A total of 639 central events were selected in this vertex range.

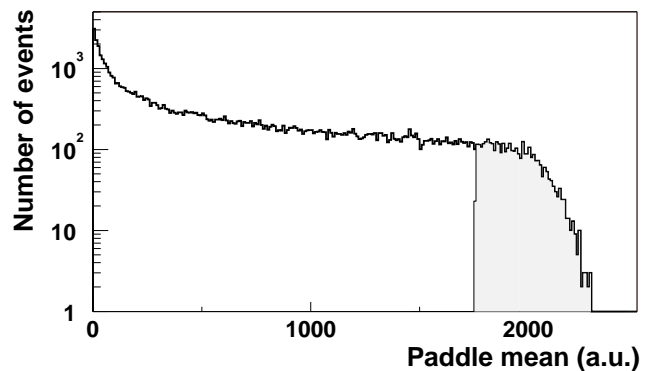


FIG. 2. Paddle signal distribution for Au+Au events at  $\sqrt{s_{NN}} = 200$  GeV. The shaded area indicates the region selected by the 6% centrality cut.

The charged particle pseudorapidity density was determined using four independent methods, which have been discussed in detail in previous publications [6,18,19]. We used an analysis of two-hit combinations (tracklets) in SPEC and VTX detectors [6,18], a hit-counting method in OCT and RING [19] and a method based on the observed energy loss in the silicon sensors (“analog method”) [19] for all subdetectors. For all four methods the multiplicity densities  $dN_{ch}/d\eta|_{|\eta|<1}$  were corrected for particles which stop in the material of the beam pipe and the first detector layer, particles from secondary interactions and feed-down products from weak decays

of neutral strange particles. The resulting systematic errors on  $dN_{ch}/d\eta|_{|\eta|<1}$  for each method at  $\sqrt{s_{NN}} = 130$  GeV are described in [6,18,19] and range from 4.5% for the SPEC tracklet analysis to 10% for the hit-counting and analog methods. MC studies showed that the systematic uncertainties are essentially the same at  $\sqrt{s_{NN}} = 200$  GeV. The combined result of all four methods is obtained using the inverse square of the estimated uncertainties as weights in the average. Based on MC studies and the comparison of all four independent multiplicity analyses, we estimate the overall systematic uncertainty of the combined result to be less than 6%. The statistical error is negligible. We obtain a primary charged particle density of  $dN_{ch}/d\eta|_{|\eta|<1} = 650 \pm 35(\text{syst})$  for the 6% most central Au+Au collisions at  $\sqrt{s_{NN}} = 200$  GeV. Normalizing per participant pair, we find  $dN_{ch}/d\eta|_{|\eta|<1}/\langle\frac{1}{2}N_{part}\rangle = 3.78 \pm 0.25(\text{syst})$ .

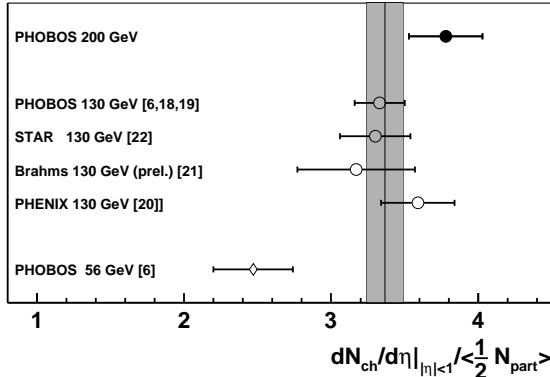


FIG. 3. Summary of RHIC results on the pseudorapidity density normalized per participant pair for central Au+Au collisions at  $\sqrt{s_{NN}} = 56, 130$  and 200 GeV. The line and grey area show the averaged result from all 4 experiments at  $\sqrt{s_{NN}} = 130$  GeV.

A compilation of all results for  $dN_{ch}/d\eta|_{|\eta|<1}/\langle\frac{1}{2}N_{part}\rangle$  in central Au+Au collisions obtained at RHIC is shown in Fig 3. It includes results from PHOBOS at  $\sqrt{s_{NN}} = 56$  GeV [6], from all four RHIC experiments at  $\sqrt{s_{NN}} = 130$  GeV [6,18–22] and our new result at  $\sqrt{s_{NN}} = 200$  GeV. The average value at 130 GeV is  $dN_{ch}/d\eta|_{|\eta|<1}/\langle\frac{1}{2}N_{part}\rangle = 3.37 \pm 0.12$ , compared to  $3.78 \pm 0.25$  reported here for 200 GeV.

In Fig. 4 the normalized yield per participant is compared to central Au+Au and Pb+Pb collisions at lower energies, including fixed target experiments [23–25]. Also shown for comparison are results from proton-antiproton ( $p\bar{p}$ ) collisions [26] and an interpolation of the  $p\bar{p}$  data. The  $dN_{ch}/d\eta$  values from E866/E917 [23] and NA49 [24,25] were obtained by integrating the measured charged particle rapidity and  $p_T$ -distributions. Within the precision of the existing data, an approximately logarithmic rise of  $dN_{ch}/d\eta|_{|\eta|<1}/\langle\frac{1}{2}N_{part}\rangle$  with  $\sqrt{s_{NN}}$  is observed over the full range of collision energies.

A direct measurement of the ratio  $R_{200/130}$  of nor-

malized multiplicity densities  $dN_{ch}/d\eta|_{|\eta|<1}/\langle\frac{1}{2}N_{part}\rangle$  at  $\sqrt{s_{NN}} = 200$  GeV and 130 GeV was also performed.

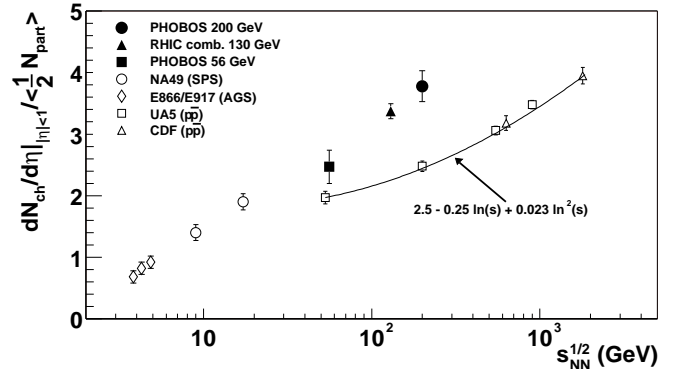


FIG. 4. Energy dependence of the pseudorapidity density normalized per participant pair for central nucleus-nucleus collisions. The data are compared with  $p\bar{p}$  data and nucleus-nucleus data from lower energies

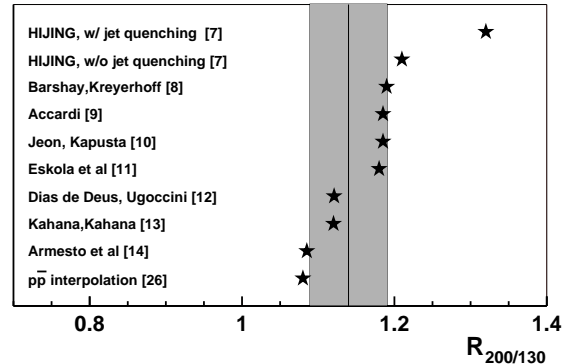


FIG. 5. Ratio  $R_{200/130}$  of pseudorapidity densities  $dN_{ch}/d\eta|_{|\eta|<1}$  at  $\sqrt{s_{NN}} = 200$  GeV and 130 GeV. The predicted increase from various models is compared to the observed increase in the data (vertical line). The grey band shows the 90% confidence interval.

The ratio was determined separately for each of the four multiplicity analyses at 130 and 200 GeV and then averaged, weighted with the inverse square of the systematic error for each ratio measurement. Many of the systematic uncertainties in each of the analyses partially cancel, leading to a significant reduction in the uncertainty of the ratio. The theoretical uncertainty in the  $N_{part}$  calculation is also largely eliminated in the ratio. We estimate that the uncertainty from the energy dependence of absorption, feed-down and acceptance corrections is less than 0.03 in  $R_{200/130}$ . Based on MC tests and the comparison of the results for the four different methods we estimate a total systematic uncertainty of less than 0.05 for the averaged result. The combined estimate of the ratio of normalized multiplicity densities  $dN_{ch}/d\eta|_{|\eta|<1}/\langle\frac{1}{2}N_{part}\rangle$  at  $\sqrt{s_{NN}} = 200$  GeV and 130 GeV, obtained from all four multiplicity analysis

methods, is  $R_{200/130} = 1.14 \pm 0.05$ . The quoted uncertainty is entirely systematic and corresponds to a 90% confidence level. In Fig. 5 this value is compared with the  $p\bar{p}$  parametrization [26] and several model calculations. The expected increase from the interpolation of  $p\bar{p}$  results falls slightly below the allowed region. Within the systematic uncertainty, the result is in agreement with most other model predictions. However, we do not observe the large increase expected in the HIJING model [7], which predicted  $R_{200/130} = 1.32$  using the default jet quenching parameters. Further theoretical work will be required to describe both the preliminary results on large  $p_T$  spectra, as well as the energy dependence of particle multiplicities.

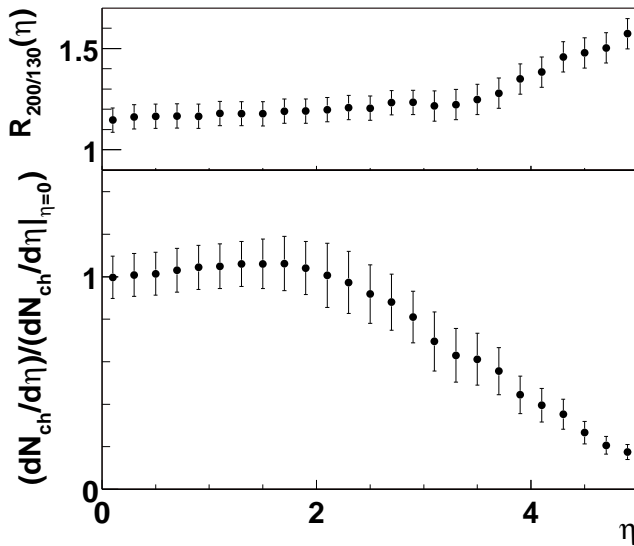


FIG. 6. The lower plot shows the shape of  $dN_{ch}/d\eta$  at  $\sqrt{s_{NN}} = 200$  GeV, obtained from the analog method, normalized to  $dN_{ch}/d\eta|_{\eta=0}$ . On top we show the pseudorapidity dependence of  $R_{200/130}$  using the result of the analog method at both energies. In both plots, the error bars indicate the systematic uncertainty.

Additional information about the change in particle production from 130 GeV to 200 GeV collision energy can be gained from Fig. 6. Using the results from the analog method [19], it shows the scaled  $dN_{ch}/d\eta$  out to  $\eta = 5$  for central collisions at 200 GeV (bottom) and the ratio of the pseudorapidity distributions at 200 and 130 GeV (top). A slow increase of the ratio is observed to  $\eta \approx 3.5$ . This is followed by a steeper rise at higher  $\eta$ , corresponding to a widening of the pseudorapidity distribution and reflecting the shift in the fragmentation region due to the larger beam rapidities at 200 GeV.

In summary, we have performed the first measurement of the pseudorapidity density of primary charged particles in Au+Au collisions at  $\sqrt{s_{NN}} = 200$  GeV. Near mid-rapidity, this density shows an approximately logarithmic evolution over a broad range of collision energies. Going from  $\sqrt{s_{NN}} = 130$  GeV to 200 GeV, the observed increase is a factor of  $1.14 \pm 0.05$ , corresponding to a moderate

increase in initial energy density. Over this energy interval, a smooth evolution of  $dN_{ch}/d\eta$  in all regions of pseudorapidity is seen. These results give further constraints for models including effects of the partonic medium in the early collision stages.

Acknowledgements: This work was partially supported by US DoE grants DE-AC02-98CH10886, DE-FG02-93ER40802, DE-FC02-94ER40818, DE-FG02-94ER40865, DE-FG02-99ER41099, W-31-109-ENG-38. NSF grants 9603486, 9722606 and 0072204. The Polish groups were partially supported by KBN grant 2 P03B 04916. The NCU group was partially supported by NSC of Taiwan under contract NSC 89-2112-M-008-024.

- [1] See *e.g.* J. P. Blaizot, Nucl. Phys. **A661**, 3c (1999).
- [2] J. D. Bjorken, Phys. Rev. **D27** 140 (1983).
- [3] M. Gyulassy and M. Plümer, Phys. Lett. **243**, 432 (1990).
- [4] J. Harris *et al.*, W. Zajc *et al.*, Proceedings of QM 2001 conference, in press.
- [5] N. Armesto and C. Pajares, Int. J. Mod. Phys. **A15**, 2019 (2000).
- [6] B. B. Back *et al.*, Phys. Rev. Lett. **85**, 3100 (2000).
- [7] X. N. Wang and M. Gyulassy, Phys. Rev. Lett. **86**, 3496 (2001).
- [8] S. Barshay, G. Kreyerhoff, hep-ph/0104303 (2001).
- [9] A. Accardi, hep-ph/0104060 (2001).
- [10] S. Jeon and J. Kapusta, Phys. Rev. C **63**, 011901 (2001).
- [11] K. J. Eskola *et al.*, hep-ph/0106330 (2001).
- [12] J. Dias de Deus and R. Ugoccioni, Phys. Lett. **B491** 253 (2000).
- [13] D. E. Kahana and S. H. Kahana, Phys. Rev. C **63**, 031901(R) (2001).
- [14] N. Armesto, C. Pajares and D. Sousa, hep-ph/0104269 (2001).
- [15] B. B. Back *et al.*, Nucl. Phys. **A661**, 690 (1999).
- [16] H. Pernegger *et al.*, Nucl. Instrum. Methods. **A419**, 549 (1998).
- [17] M. Gyulassy and X. N. Wang, Phys. Rev. **D44**, 3501 (1991).
- [18] B. B. Back *et al.*, nucl-ex/0105011.
- [19] B. B. Back *et al.*, Phys. Rev. Lett. in press, nucl-ex/0106006.
- [20] K. Adcox *et al.*, Phys. Rev. Lett. **86**, 3500 (2001).
- [21] F. Videbaek *et al.*, Proceedings of QM 2001 conference, in press.
- [22] C. Adler *et al.*, nucl-ex/0106004 (2001).
- [23] L. Ahle *et al.*, Phys. Lett. B **476**, 1 (2000); L. Ahle *et al.*, Phys. Lett. B **490** 53 (2000); B. B. Back *et al.*, Phys. Rev. Lett. **86**, 1970 (2001).
- [24] J. Bächler *et al.*, Nucl. Phys. **A661** 45 (1999)
- [25] C. Blume *et al.*, Proceedings of QM 2001 conference, in press.
- [26] F. Abe *et al.*, Phys. Rev. **D41** 2330 (1990).